Article

End-Cap Effects on Vibrational Structures of Finite-Length Carbon Nanotubes

Takashi Yumura, Daijirou Nozaki, Shunji Bandow, Kazunari Yoshizawa, and Sumio Iijima

J. Am. Chem. Soc., **2005**, 127 (33), 11769-11776• DOI: 10.1021/ja0522579 • Publication Date (Web): 30 July 2005

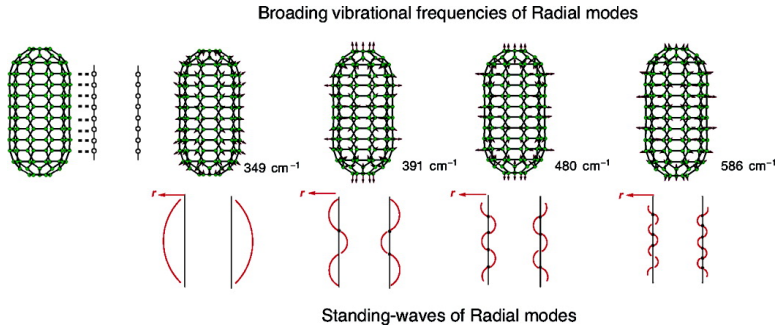

More About This Article

Additional resources and features associated with this article are available within the HTML version:

- Supporting Information
- Links to the 6 articles that cite this article, as of the time of this article download
- Access to high resolution figures
- Links to articles and content related to this article
- Copyright permission to reproduce figures and/or text from this article

View the Full Text HTML

J|A|C|S
ARTICLES
Published on Web 07/30/2005

End-Cap Effects on Vibrational Structures of Finite-Length Carbon Nanotubes

Takashi Yumura,*[,†,‡] Daijirou Nozaki,[§] Shunji Bandow,[‡] Kazunari Yoshizawa,[§] and Sumio Iijima[†,‡]

Contribution from the Research Center for Advanced Carbon Materials, National Institute of Advanced Industrial Science and Technology (AIST), Tsukuba 305-8565, Japan, Department of Materials Science and Engineering, Meijo University, Tenpaku-ku, Nagoya 468-8502, Japan, and Institute for Materials Chemistry and Engineering, Kyushu University, Higashi-ku, Fukuoka 812-8581, Japan

Received April 7, 2005; E-mail: t-yumura@aist.go.jp

Abstract: Vibrational structures of C_{60}-related finite-length nanotubes, C_{40+20n} and C_{42+18n} ($1 \le n \le 4$), in which n is, respectively, the number of cyclic *cis*- and *trans*-polyene chains inserted between fullerene hemispheres, are analyzed from density functional theory (DFT) calculations. To illuminate the end-cap effects on their vibrational structures, the corresponding tubes terminated by H atoms $C_{20n}H_{20}$ and $C_{18n}H_{18}$ ($1 \le n \le 5$) are also investigated. DFT calculations show a broad range of vibrational frequencies for the finite-size nanotubes: high-frequency modes (1100−1600 cm^{-1}) containing oscillations along tangential directions (tangential modes), medium-frequency modes (700−850 cm^{-1}) whose oscillations are located on the edges or end caps, and low-frequency modes (300−600 cm^{-1}) involving oscillations along the radial directions (radial modes). Broadening of the calculated frequencies is due to the number of nodes in the standing waves of normal modes in the finite-size tubes. In the capped tubes, calculated vibrational frequencies are insensitive to the number of chains (n), whereas in the uncapped tubes, most vibrational frequencies change significantly with an increase in tube length. The discrepancy in the size dependency is reasonably understood by their C−C bonding networks; the capped tubes have similar bond-length alternation patterns within the polyene chains irrespective of n, whereas the uncapped tubes have various bond-deformation patterns. Thus, DFT calculations illuminate that the edge effects have strong impacts on the vibrational frequencies in the finite-size nanotubes.

Introduction

Single-walled carbon nanotubes (SWNTs) that consist of a graphene sheet wrapped to form a cylinder[1,2] are on the order of several nanometers in diameter but several microns in length. Because of their high aspect ratio, the tubes can be viewed as a quasi-one-dimensional system.[3] The structures of SWNTs are represented by a chiral vector $C = na_1 + ma_2$, where a_1 and a_2 denote equivalent lattice vectors of the graphene sheet. Depending on their chirality (n, m) and the tube diameter, SWNTs become metallic or semiconducting.[1,2] Despite their promising structures as components in submicrometer-scale devices, controlling nanotube length is of interest for various applications in nanometer-scale devices.[4−6] Venema et al. presented a technique to cut nanotubes into shorter sections with a few nanometers using a scanning tunneling microscope (STM).[4a] Limiting the length of one-dimensional systems results in a "particle-in-a-box" quantization of its energy levels, and therefore, electronic properties of short nanotubes are dependent on their length.[4−6]

Shorter nanotubes are also generated inside a SWNT by heating "C_{60} peapods",[7] where the C_{60} molecules are encapsulated in a SWNT.[8] According to transmission electronic

[†] AIST.
[‡] Meijo University.
[§] Kyushu University.

(1) Iijima, S. *Nature* **1991**, *354*, 56.
(2) Iijima, S.; Ichihashi, T. *Nature* **1993**, *363*, 603.
(3) (a) Saito, R.; Fujita, M.; Dresselhaus, G.; Dresselhaus, M. S. *Appl. Phys. Lett.* **1992**, *60*, 2204. (b) Dresselhaus, M. S.; Dresselhaus, G.; Saito, R. *Phys. Rev. B* **1992**, *45*, 6234. (c) Dresselhaus, M. S.; Dresselhaus, G.; Eklund, R. C. *Science of Fullerenes and Carbon Nanotubes*; Academic Press: New York, 1996. (d) Saito, R.; Dresselhaus, G.; Dresselhaus, M. S. *Physical Properties of Carbon Nanotubes*; Imperial College Press: London, 1998.
(4) (a) Venema, L. C.; Wildöer, J. W. G.; Temminck Tuinstra, H. J. L.; Dekker, C.; Rinzler, A. G.; Smalley, R. E. *Appl. Phys. Lett.* **1997**, *71*, 2629. (b) Venema, L. C.; Wildöer, J. W. G.; Janssen, J. W.; Tan, S. J.; Temminck Tuinstra, H. J. L.; Kouwenhoven, L. P.; Dekker, C. *Science* **1999**, *283*, 52. (c) Rubio, A.; Apell, S. P.; Venema, L. C.; Dekker, C. *Eur. Phys. J. B* **2000**, *17*, 301.
(5) Rubio, A.; Sánchez-Portal, D.; Artacho, E.; Ordejón, R.; Soler, J. M. *Phys. Rev. Lett.* **1999**, *82*, 3520.
(6) Odom, T. W.; Huang, J.-L.; Kim, P.; Lieber, C. M. *J. Phys. Chem. B* **2000**, *104*, 2794.
(7) (a) Bandow, S.; Takizawa, M.; Hirahara, K.; Yudasaka, M.; Iijima, S. *Chem. Phys. Lett.* **2001**, *337*, 48. (b) Bandow, S.; Takizawa, M.; Kato, H.; Okazaki, T.; Shinohara, H.; Iijima, S. *Chem. Phys. Lett.* **2001**, *347*, 23. (c) Bandow, S.; Hiraoka, T.; Yumura, T.; Hirahara, K.; Iijima, S. *Chem. Phys. Lett.* **2003**, *384*, 320. (d) Yumura, T.; Hirahara, K.; Bandow, S.; Yoshizawa, K.; Iijima, S. *Chem. Phys. Lett.* **2004**, *386*, 38.
(8) (a) Smith, B. W.; Monthioux, M.; Luzzi, D. E. *Nature* **1998**, *396*, 323. (b) Smith, B. W.; Monthioux, M.; Luzzi, D. E. *Chem. Phys. Lett.* **1999**, *315*, 31. (c) Smith, B. W.; Luzzi, D. E. *Chem. Phys. Lett.* **2000**, *321*, 169.

10.1021/ja0522579 CCC: $30.25

Chart 1

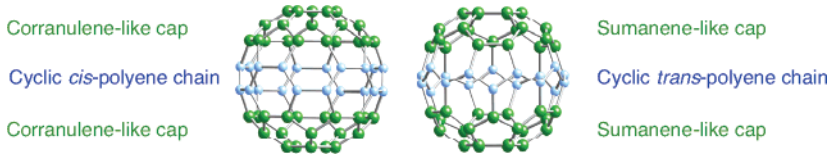

microscopy (TEM) observations, the tubes capped with fullerene hemispheres have lengths of 13.7 and 21.2 Å when they consist of three and four C_{60} molecules in size, respectively.[7] End-cap effects as well as finite-size effects should play an essential role in determining their electronic and geometrical properties. The electronic properties of capped[9−12] and uncapped[13−15] nanotubes have been analyzed using various theoretical methodologies. In a previous study, we investigated from density functional theory (DFT) calculations the geometries of the finite-length (5,5) armchair and (9,0) zigzag nanotubes capped with fullerene hemispheres and those of the corresponding nanotubes terminated by H atoms.[12] The DFT calculations show that the capped and uncapped nanotubes adopt different bond-length alternation patterns; the capped tubes have similar bond-length alternation patterns within the polyene chains irrespective of tube length, whereas the uncapped tubes have various bond-deformation patterns. An orbital interaction analysis reveals that the similar bond-length alternation patterns come from interactions of the cylindrical segment with the fullerene hemispheres in the capped nanotubes.[12] Hence, the fullerene hemispheres are responsible for the geometrical features in the finite-length achiral nanotubes.

It is important to analyze their vibrational structures in the capped nanotubes, which can be generated during the C_{60} coalescence inside the SWNT.[16] They are observable using Raman and infrared (IR) spectroscopy, in principle. In fact, vibrational spectra of infinite-length nanotubes have been detected by resonance Raman spectroscopy.[17,18] Radial breathing modes (RBM) and tangential G-band modes are known to have strong Raman intensities in lower (100−450 cm^{-1}) and higher (1500−1600 cm^{-1}) frequency regions, respectively.[18] However, the infinite-length nanotubes have no Raman peak in an intermediate-frequency region (500−1200 cm^{-1}) according to theoretical calculations.[18] Saito et al. revealed using nonresonant bond polarization theory that the finite-length (10,10) armchair nanotube without any termination has Raman intensities in the intermediate-frequency region.[19] The intermediate-frequency modes correspond to A_{1g} *z*-directed modes, whose vibrations are along the tube (*z*) axis.

Their suggestions are useful for understanding the intermediate-frequency modes observed experimentally. However, our knowledge of the role of the fullerene hemisphere in the vibrational structures is still lacking. The importance of the fullerene hemispheres in the geometries of the finite-length nanotubes implies that the end caps should have strong impact on their vibrational frequencies. In the present paper, we report vibrational analyses of C_{60}-related tubes to illuminate the end-cap effects on their vibrational structures.

Finite-Length Carbon Nanotubes Related to C_{60}. As shown in Chart 1, C_{60} can be partitioned into one cyclic *cis*-polyene chain with 20 carbon atoms and two corranulene-like caps along a C_5 rotation axis. It can also be viewed as one cyclic *trans*-polyene chain with 18 carbon atoms and two sumanene-like caps along a C_3 rotation axis. When cyclic *cis*-polyene chains are inserted between the caps along the C_5 rotation axis, the tubes C_{40+20n} with D_{5d} symmetry are formed, where *n* is the number of chains inserted. In a similar sense, increasing the number of *trans*-polyene chains between the caps leads to the formation of the tubes C_{42+18n}. The tubes capped with the fullerene hemispheres are between C_{60} and the infinite-length (5,5) armchair or (9,0) zigzag nanotubes. We also consider the corresponding tubes terminated by H atoms ($C_{20n}H_{20}$ and $C_{18n}H_{18}$). The H-atom-terminated tubes $C_{20n}H_{20}$ have a relevance to a hoop-shaped benzenoid [10]cyclophenacene around the equator of $C_{60}(CH_3)_5(C_6H_5)_5H_2$ because the calculated geometry of $C_{40}H_{20}$ well reproduces their C−C bond networks obtained from the X-ray crystallographic analysis.[20] Thus, it is also important to elucidate the vibrational structures of the uncapped tubes in themselves. In the present study, we analyze the vibrational structures of the tubes C_{40+20n}, C_{42+18n}, $C_{20n}H_{20}$, and $C_{18n}H_{18}$ from DFT B3LYP calculations. Throughout the study, we pay attention to the cylindrical segments in the tubes, which can be regarded as consisting of certain numbers (*n*) of cyclic polyene chains.

Method of Calculation. We carried out quantum chemical calculations on the basis of the hybrid Hartree−Fock/density functional theory (B3LYP) method[21,22] using the Gaussian 03 program package.[23] The B3LYP method consists of the Slater exchange, the Hartree−Fock exchange, the exchange functional of Becke,[21] the correlation functional of Lee, Yang, and Parr (LYP),[22] and the correlation functional of Vosko, Wilk, and Nusair (VWN).[24] The basis set we used for the C and H atoms is 6-31G*.[25,26] The geometries of C_{40+20n}, C_{42+18n}, $C_{20n}H_{20}$, and

(9) Harigaya, K. *Phys. Rev. B* **1992**, *45*, 12071.
(10) Sato, T.; Tanaka, M.; Yamabe, T. *Synth. Met.* **1999**, *103*, 2525.
(11) Cioslowski, J.; Rao, N.; Moncrieff, D. *J. Am. Chem. Soc.* **2002**, *124*, 8485.
(12) Yumura, T.; Bandow, S.; Yoshizawa, K.; Iijima, S. *J. Phys. Chem. B* **2004**, *108*, 11426.
(13) Rochefort, A.; Salahub, D. R.; Avouris, P. *J. Phys. Chem. B* **1999**, *103*, 641.
(14) Matsuo, Y.; Tahara, K.; Nakamura, E. *Org. Lett.* **2003**, *5*, 3181.
(15) Zhou, Z.; Steigerwald, M.; Hybertsen, M.; Brus, L.; Friesner, R. A. *J. Am. Chem. Soc.* **2004**, *126*, 3597.
(16) Han, S.; Yoon, M.; Berber, S.; Park, N.; Osawa, E.; Ihm, J.; Tománek, D. *Phys. Rev. B* **2004**, *70*, 113402.
(17) Rao, A. M.; Richter, E.; Bandow, S.; Chase, B.; Eklund, P. C.; Williams, K. A.; Fang, S.; Subbaswamy, K. R.; Menon, M.; Thess, A.; Smalley, R. E.; Dresselhaus, G.; Dresselhaus, M. S. *Science* **1997**, *275*, 187.
(18) (a) Dresselhaus, M. S.; Dresselhaus, G.; Jorio, A.; Filho, A. G. S.; Pimenta, M. A.; Saito, R. *Acc. Chem. Res.* **2002**, *35*, 1070. (b) Dresselhaus, M. S.; Dresselhaus, G.; Jorio, A.; Filho, A. G. S.; Saito, R. *Carbon* **2002**, *40*, 2043.
(19) Saito, R.; Takeya, T.; Kimura, T.; Dresselhaus, G.; Dresselhaus, M. S. *Phys. Rev. B* **1999**, *59*, 2388.
(20) Nakamura, E.; Tahara, K.; Matsuo, Y.; Sawamura, M. *J. Am. Chem. Soc.* **2003**, *125*, 2834.
(21) (a) Becke, A. D. *Phys. Rev. A* **1988**, *38*, 3098. (b) Becke, A. D. *J. Chem. Phys.* **1993**, *98*, 5648. (c) Stephens, P. J.; Devlin, F. J.; Chabalowski, C. F.; Frisch, M. J. *J. Phys. Chem.* **1994**, *98*, 11623.
(22) Lee, C.; Yang, W.; Parr, R. G. *Phys. Rev. B* **1988**, *37*, 785.
(23) Frisch, M. J. et al. *Gaussian 03*; Gaussian, Inc.: Pittsburgh, PA, 2003.
(24) Vosko, S. H.; Wilk, L.; Nusair, M. *Can. J. Phys.* **1980**, *58*, 1200.
(25) (a) Ditchfield, R.; Hehre, W. J.; Pople, J. A. *J. Chem. Phys.* **1971**, *54*, 724. (b) Hehre, W. J.; Ditchfield, R.; Pople, J. A. *J. Chem. Phys.* **1972**, *56*, 2257.
(26) Hariharan, P. C.; Pople, J. A. *Theor. Chim. Acta* **1973**, *28*, 213.

Table 1. Calculated Vibrational Frequencies for Labeled and Unlabeled C_{60} Molecules[a]

species	C_{60}			$^{13}C_{60}$			$^{12}C_{40}{}^{13}C_{20}$		$^{12}C_{42}{}^{13}C_{18}$		
	A_g	H_g	G_g	A_g A_g	H_g H_g	G_g G_g	A_{1g} A_g	A_{1g} H_g	A_{1g} A_g	A_{1g} H_g	A_{1g} G_g
symmetry labels	487	262	483	468 (19)	252 (10)	464 (19)	481 (6)	257 (5)	485 (2)	259 (3)	473 (10)
frequency (cm^{-1})	1475	432	567	1417 (58)	415 (17)	545 (22)	1462 (13)	425 (7)	1461 (14)	427 (5)	557 (10)
		708	743		680 (28)	713 (30)		705 (3)		687 (21)	738 (5)
		774	1074		743 (31)	1032 (42)		767 (7)		770 (4)	1070 (4)
		1107	1311		1063 (44)	1259 (52)		1089 (18)		1095 (12)	1283 (28)
		1253	1510		1203 (50)	1450 (60)		1226 (27)		1243 (10)	1498 (12)
		1428			1372 (56)			1389 (39)		1401 (27)	
		1588			1525 (63)			1578 (10)		1546 (42)	

[a] The values in parentheses are isotope shifts upon ^{13}C substitution. The vibrational symmetry labels denoted in the third column represent irreducible representations of the corresponding vibrational modes for unlabeled C_{60}.

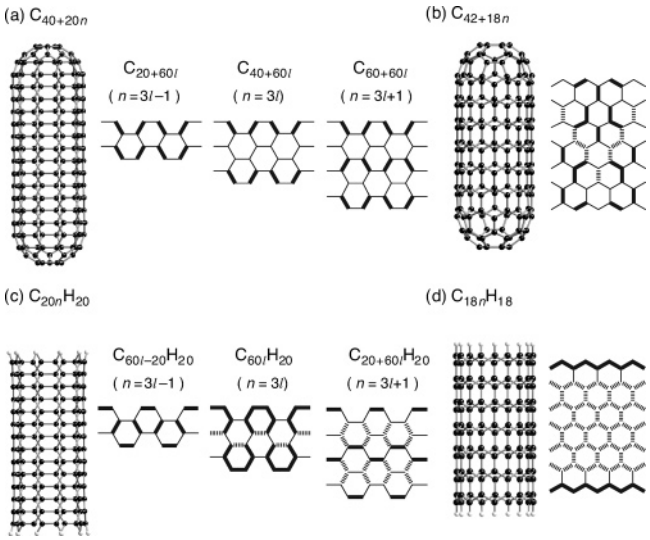

Figure 1. Bond-deformation patterns in the cylindrical segments of (a) C_{40+20n}, (b) C_{42+18n}, (c) $C_{20n}H_{20}$, and (d) $C_{18n}H_{18}$. The bold lines indicate C−C bonds shorter than 1.42 Å, the broken lines are those falling in the range of 1.421−1.430 Å, and the single lines those larger than 1.431 Å.

$C_{18n}H_{18}$ were optimized, and the harmonic vibrational frequencies were calculated by the analytical evaluation of the second derivatives of energy with respect to nuclear displacement. The finite-length nanotubes C_{40+20n}, C_{42+18n}, $C_{20n}H_{20}$, and $C_{18n}H_{18}$ have $112 + 60n$, $120 + 54n$, $54 + 60n$, and $48 + 54n$ vibrational degrees of freedom, respectively. The Hartree−Fock (HF) method is known to systematically overestimate fundamental frequencies by 10−15% because of the neglect of electron correlation,[27a] while the B3LYP method reasonably estimates fundamental frequencies within an accuracy of 2−3%.[27] In this study, we used a uniform scaling factor of 0.9806 on calculated frequencies obtained at the B3LYP/6-31G* level of theory.[28]

Results and Discussion

Geometrical Features of the Finite-Length Nanotubes. Before discussing the vibrational structures of C_{40+20n}, C_{42+18n}, $C_{20n}H_{20}$, and $C_{18n}H_{18}$, let us first overview the end-cap effects on the geometries of the tubes. We see in Figure 1 bond-length alternation patterns of the polyene chains concerning their cylindrical segments in the finite-length nanotubes, where the thick lines indicate C−C bonds shorter than 1.42 Å, the broken lines those falling in the range of 1.421−1.430 Å, and the single lines those larger than 1.431 Å. As shown in Figure 1, C_{40+20n} can be classified into three types. They have at least one *cis*-polyene chain with a bond-length alternate pattern, in which the C−C bonds along the tube axis are contracted while the C−C bonds around the chain are elongated. In C_{40+60l} ($n = 3l$, where l is integer), a single *cis*-polyene chain is located on each edge of the cylinder; however, bond-length alternating chains are distributed throughout the cylinder of C_{20+60l} ($n = 3l - 1$). C_{60+60l} ($n = 3l + 1$) have bonding networks between C_{20+60l} and C_{40+60l}, where two *cis*-polyene chains are connected by one carbon belt lying in a plane perpendicular to the tube axis. Despite the same bond-length alternation pattern within the chains in the capped armchair nanotube, there are various bond-deformation patterns in the uncapped tubes, in which bonding networks can be classified into three subgroups; the structures of $C_{60l-20}H_{20}$, $C_{60l}H_{20}$, and $C_{20+60l}H_{20}$ show, respectively, Kekulé, complete Clar, and incomplete Clar networks.[14] This is an interesting nanometer-sized electronic effect that cannot be observed in infinite-length nanotubes.[29] Similarly, the bond-deformation patterns of cyclic *trans*-polyene chains in the C_{42+18n} series are different from those in $C_{18n}H_{18}$ series; the C_{42+18n} series exhibit Kekulé-type networks, while $C_{18n}H_{18}$ series exhibit complete Clar structures. The difference in the bond-deformation patterns between the capped and uncapped nanotubes is understandable from orbital interactions of the cylindrical segment with fullerene hemispheres.[12] Thus, the end caps play an important role in determining the bond-length alternation

Table 2. Calculated Vibrational Frequencies of Isotope-Labeled C_{60}, $C_{20}H_{20}$, and $C_{18}H_{18}$[a]

species	$C_{20}H_{20}$	$^{13}C_{20}H_{20}$	$C_{18}H_{18}$	$^{13}C_{18}H_{18}$
	A_{1g}	A_{1g}	A_{1g}	A_{1g}
symmetry labels	192	185 (7)	231	224 (7)
frequency (cm^{-1})	647	645 (2)	314	303 (11)
	890	859 (31)	396	386 (10)
	1283	1274 (9)	854	841 (13)
	1656	1598 (58)	1064	1060 (4)
	3101	3091 (10)	1280	1265 (15)
			1286	1239 (47)
			1581	1533 (48)
			3085	3076 (9)
			3086	3077 (9)

[a] The values in parentheses are isotope shifts upon ^{13}C substitution.

(27) Scott, A. P.; Radom, L. *J. Phys. Chem.* **1996**, *100*, 16502.
(28) Halls, M. D.; Velkovski, J.; Schlegel, H. B. *Theor. Chem. Acc.* **2001**, *105*, 413.
(29) (a) Sun, G.; Kürti, J.; Kertesz, M.; Baughman, R. H. *J. Phys. Chem. B* **2003**, *107*, 6924. (b) Sun, G.; Kürti, J.; Kertesz, M.; Baughman, R. H. *J. Am. Chem. Soc.* **2002**, *124*, 15076.

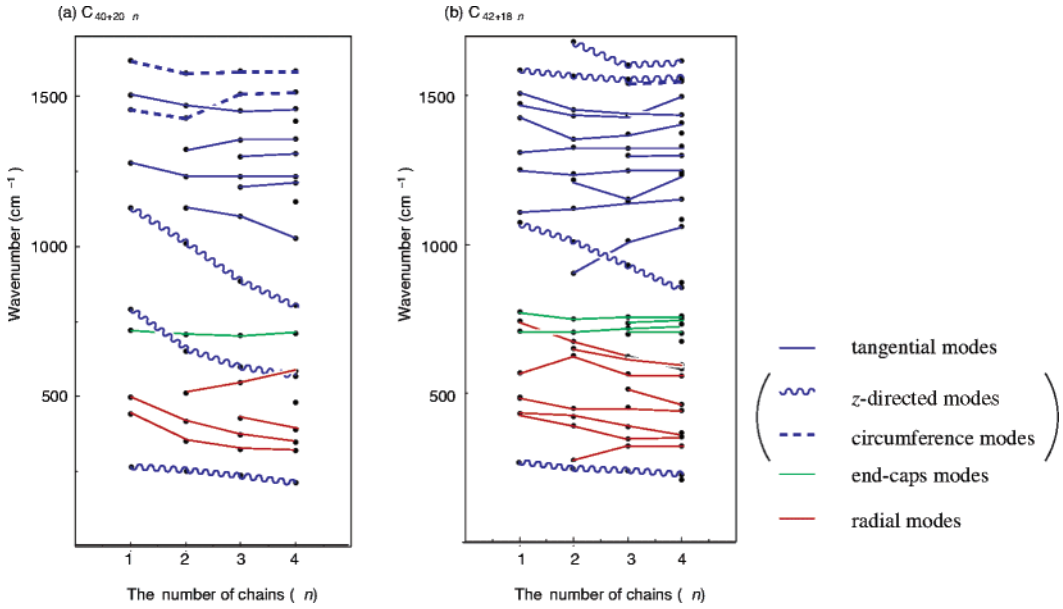

Figure 2. Calculated vibrational frequencies as a function of the number of chains (n) involved in (a) C_{40+20n} and (b) C_{42+18n}. The blue, green, and red lines represent the tangential, end caps, and radical modes, respectively. Among the tangential modes, the z-directed and circumference modes are also expressed by wavy and broken lines, respectively.

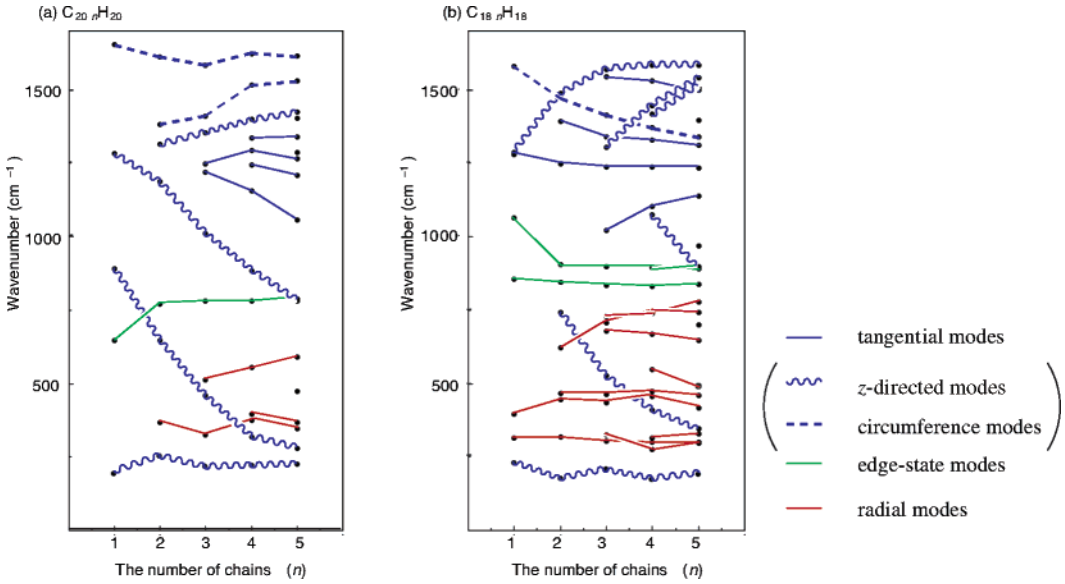

Figure 3. Calculated vibrational frequencies as a function of the number of chains (n) involved in (a) $C_{20n}H_{20}$ and (b) $C_{18n}H_{18}$. The blue, green, and red lines represent the tangential, edge state, and radical modes, respectively. Among the tangential modes, the z-directed and circumference modes are also expressed by wavy and broken lines, respectively.

patterns in the tubes. On the basis of these findings, we analyze in detail the vibrational structures of the finite-length armchair and zigzag nanotubes in the next section.

Vibrational Structures of the Finite-Length Nanotubes C_{60}, $C_{20}H_{20}$, and $C_{18}H_{18}$. According to the group theory, the vibrational modes of C_{60} can be classified as follows

$$\Gamma(C_{60}) = 2A_g + 3T_{1g} + 4T_{2g} + 6G_g + 8H_g + A_u + 4T_{1u} + 5T_{2u} + 6G_u + 7H_u$$

Table 1 lists calculated vibrational frequencies of the A_g, H_g, and G_g vibrational modes, and the values in parentheses are isotope shifts of labeled molecules. The A_g and H_g modes are Raman-active. Since the calculated values in Table 1 well reproduce those obtained from the Raman spectrum,[30] B3LYP harmonic frequencies provide reliable theoretical vibrational spectra in the carbon systems. The C_{60} molecule exhibits low- and high-frequency vibrational modes, which are assigned to radial and tangential motions, respectively.[3,31,32] For example,

(30) The experimental Raman frequencies are 496 ± 2 (A_g), 1470 ± 2 (A_g), 271 ± 2 (H_g), 433 ± 3 (H_g), 710 ± 2 (H_g), 774 ± 2 (H_g), 1099 ± 2 (H_g), 1250 ± 2 (H_g), 1426 ± 2 (H_g), and 1575 ± 3 (H_g) from ref 2c.

(31) (a) Eklund, P. C.; Zhou, R.; Wang, K.-A.; Dresselhaus, G.; Dresselhaus, M. S. *J. Phys. Chem. Solids* **1992**, *53*, 1391. (b) Dong, Z.-H.; Zhou, P.; Holden, J. M.; Eklund, P. C.; Dresselhaus, G.; Dresselhaus, M. S. *Phys. Rev. B* **1993**, *48*, 2862. (c) Wang, K.-A.; Rao, A. M.; Eklund, P. C.; Dresselhaus, G.; Dresselhaus, M. S. *Phys. Rev. B* **1993**, *48*, 11376. (d) Martin, M.; Fabian, J.; Godard, J.; Bernier, P.; Lambert, J. M.; Mihaly, L. *Phys. Rev. B* **1995**, *51*, 2844. (e) Guha, S.; Menéndez, J.; Page, J. B.; Adams, G. B. *Phys. Rev. B* **1997**, *56*, 15431. (f) Guha, S.; Menéndez, J.; Page, J. B.; Adams, G. B. *Phys. Rev. B* **1997**, *56*, 15431.

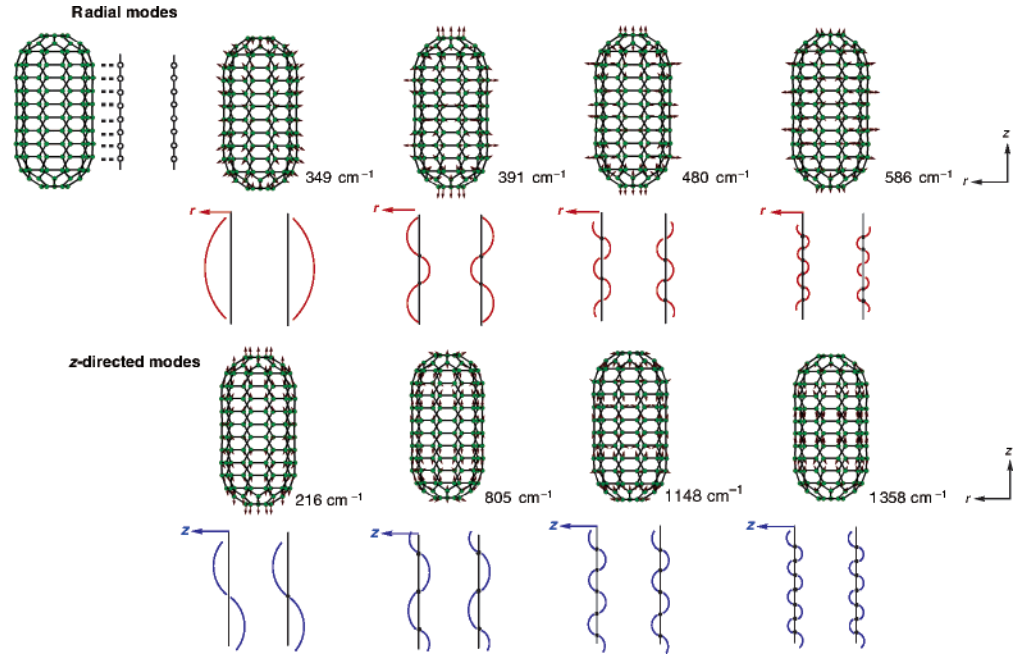

Figure 4. Nodal characters in vibrational modes of C_{120}. Amplitudes of motions along the radial directions and the tube (z) axis are represented by red and blue lines, respectively.

Chart 2

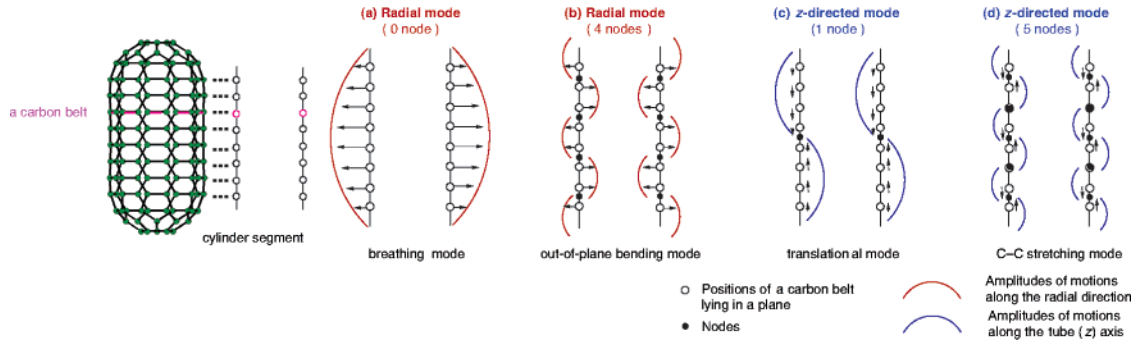

the mode at 487 cm^{-1} is a radial breathing mode, and the mode at 1475 cm^{-1} is a pentagonal pinch mode.

Let us next look at vibrational modes of isotope-labeled C_{60} molecules in order to increase our understanding of the C_{60} vibrational modes. Here, we consider the totally symmetric modes of the isotope species $^{12}C_{40}{}^{13}C_{20}$ (D_{5d} symmetry) and $^{12}C_{42}{}^{13}C_{18}$ (D_{3d} symmetry), where the ^{12}C atoms in a single polyene chain of C_{60} are replaced with ^{13}C atoms, which are denoted by blue in Chart 1. Calculated vibrational frequencies for the isotope-labeled C_{60} molecules are listed in Table 1, and their vibrational modes are visualized in Figure S1 (Supporting Information). The lowering of the I_h symmetry causes splittings of their degenerate vibrational modes of C_{60}. In fact, the A_{1g} modes of $^{12}C_{40}{}^{13}C_{20}$ come from the splittings of the A_g and H_g modes of C_{60}, and those of $^{12}C_{42}{}^{13}C_{18}$ come from the splittings of the A_g, H_g, and G_g modes. Although the ^{13}C isotope labelings decrease most frequencies, some vibrational frequencies are insensitive to the ^{13}C isotope labelings. As shown in Table 1, the wavenumbers 708, 774, 1475, and 1588 cm^{-1} show almost no change upon ^{13}C substitution along the C_5 rotation axis; the values ω_{13}/ω_{12} were calculated to be ~0.99, being larger than those in $^{13}C_{60}$ (0.96),[33] where ω_{12} and ω_{13} are calculated vibrational frequencies for the unlabeled and labeled C_{60} molecules, respectively. There are also ^{13}C isotope insensitive modes along the C_3 rotation axis at 743, 774, 1074, 1253, and 1510 cm^{-1}. Since the ^{13}C atoms are on the single *cis*-polyene chain of C_{60} or are on the single *trans*-polyene chain, the ^{13}C isotope insensitive modes are derived from oscillations located on the end caps. The isotope labeling indicates that C_{60} has modes associated with vibrations on the end caps along the C_5 and C_3 rotation axes at 708 and 743 cm^{-1}, respectively. The mode at 708 (743) cm^{-1} is H_g (G_g). $C_{20}H_{20}$ and $C_{18}H_{18}$ also have ^{13}C-insensitive frequency modes, as shown in Table 2. The modes at 647, 1283, and 3101 cm^{-1} in $C_{20}H_{20}$ and the modes at 854, 1064, 1280, 3085, and 3086 cm^{-1} in $C_{18}H_{18}$ are also insensitive. Despite absence of the fullerene hemispheres, $C_{20}H_{20}$ ($C_{18}H_{18}$) also has a ^{13}C-insensitive mode in the intermediate-frequency region at 647 (854) cm^{-1}.

(32) (a) Negri, F.; Orlandi, G.; Zerbetto, F. *Chem. Phys. Lett.* **1988**, *144*, 31. (b) Stanton, R. E.; Newton, M. D. *J. Phys. Chem.* **1988**, *92*, 2141. (c) Jishi, R. A.; Mirie, R. M.; Dresselhaus, M. S. *Phys. Rev. B* **1992**, *45*, 13685. (d) Giannozzi, P.; Baroni, S. *J. Chem. Phys.* **1994**, *100*, 8537. (e) Schettino, V.; Salvi, P. R.; Bini, R.; Cardini, *J. Chem. Phys.* **1994**, *101*, 11079. (f) Choi, C. H.; Kertesz, M.; Mihaly, L. *J. Phys. Chem. A* **2000**, *104*, 102. (g) Schettino, V.; Pagliai, M.; Ciabini, L.; Cardini, G. *J. Phys. Chem. A* **2001**, *105*, 11192.

(33) The values ω_{13}/ω_{12} are always nearly constant to be 0.96, which corresponds to $\sqrt{12/13}$.

Size Dependence of Frequencies for Finite-Length Nanotubes. In this section, we focus our discussion on the calculated vibrational frequencies for the capped nanotubes C_{40+20n} and C_{42+18n}, and the uncapped nanotubes $C_{20n}H_{20}$ and $C_{18n}H_{18}$. The A_{1g} vibrational frequencies for the capped and uncapped tubes are given as a function of the number of chains (n) in Figures 2 and 3, respectively. Their vibrational modes and calculated frequencies are shown in Figures S2−S5 (Supporting Information). In Figures 2 and 3, we connect suitable dots with a line, based on their vibrational patterns together with calculated isotope shifts upon ^{13}C substitutions in the cylinder segments. Depending on the number of chains involved in the tubes, a broad range of calculated frequencies is obtained in the finite-length nanotubes relative to infinite-length nanotubes; the high-frequency modes (1100−1600 cm^{-1}) composed of oscillations along tangential directions in the tubes (tangential modes), the medium-frequency modes (700−850 cm^{-1}) whose oscillations are located on the edges or end caps, and the low-frequency modes (300−600 cm^{-1}) involving oscillations along the radial directions (radial modes), which are shown in blue, green, and red lines, respectively, in Figures 2 and 3. The tangential vibrations on a wrapped graphene sheet are formed by combinations of vibrations along the rotation (z) axis (z-directed modes that are presented by wavy lines in Figures 2 and 3) and perpendicular to the axis (circumference modes that are presented by broken lines). Figures S2−S5 show that the tangential modes can be classified into three subgroups: C−C stretching modes (1400−1600 cm^{-1}), Kekulé modes (1380 cm^{-1}) where C−C bonds are compressed and stretched alternatively, and C−C−C bending modes (1100−1250 cm^{-1}).

Broadening of the calculated frequencies is due to the number of nodes in the standing waves of normal modes in the finite-size tubes, as shown in Figures S2−S5. Their vibrational patterns are schematically represented in Figure 4 and Chart 2. We can see in Figure 4 (Chart 2) that there is a nice analogy between these patterns and normal modes of a line of n-coupled oscillators whose amplitudes are given by a sine wave. For example, the radial mode at 349 cm^{-1} has no node with respect to the tube length in C_{120} (r-breathing mode), whereas there are four nodes along the rotation axis in the mode at 480 cm^{-1}. The directions of oscillations are reversed around the nodes, and hence, its vibrational pattern assumes out-of-plane bending characters. Increasing the number of nodes in the radial modes,[34] the modes enhance the bending characters, and their frequencies become high. These features are also seen in the tangential modes along the tube (z) axis (z-directed modes). We see in Chart 2c (Chart 2d) that the z-directed modes have translational (C−C stretching) vibrations when the number of nodes is small (large). Hence, the z-directed modes have high frequencies with an increase in the number of nodes. The calculated frequencies of the z-directed modes fall in a wide range of 216−1358 cm^{-1} relative to those of the radial modes (349−586 cm^{-1}).

Next, we discuss in detail the vibrational frequencies for the capped tubes, C_{40+20n} and C_{42+18n}. Figure 2 shows that most frequencies for the capped nanotubes do not change irrespective of tube length, especially the high-frequency modes (above 1250 cm^{-1}) and the intermediate-frequency modes (∼700 cm^{-1}). The size-insensitive modes in the high-frequency regions are associated with the tangential modes. Among the tangential modes, the armchair and zigzag series show different tendencies in the calculated frequencies; frequencies of the circumference C−C stretching (1580 cm^{-1}) in the armchair series are higher than those of the z-directed C−C stretching (1350 cm^{-1}), whereas in the zigzag series, the z-directed modes have higher frequencies (∼1600 cm^{-1}). In contrast, the intermediate-frequency modes consist of oscillations on the end caps in the armchair and zigzag series. The calculated frequency in the armchair (zigzag) series has a nearly constant value of ∼708 cm^{-1} (∼743 cm^{-1}), which is essentially identical to that of the H_g (G_g) mode of C_{60}. Hence, the size-insensitive vibrational modes at ∼700 cm^{-1} are characteristic in the C_{60}-related nanotubes. In the C_{40+20n} (C_{42+18n}) series, only the z-directed mode frequency fluctuates sensitively, ranging from 805 (855) to 1107 (1074) cm^{-1}.

On the contrary to the capped tubes, most vibrational frequencies remarkably change as a function of the number of chains (n) in the uncapped tubes, $C_{20n}H_{20}$ and $C_{18n}H_{18}$, as shown in Figure 3. In the uncapped nanotubes, enlargement of the tube lengths causes a significant frequency change in the tangential mode, which is larger than those of the edge state and radial

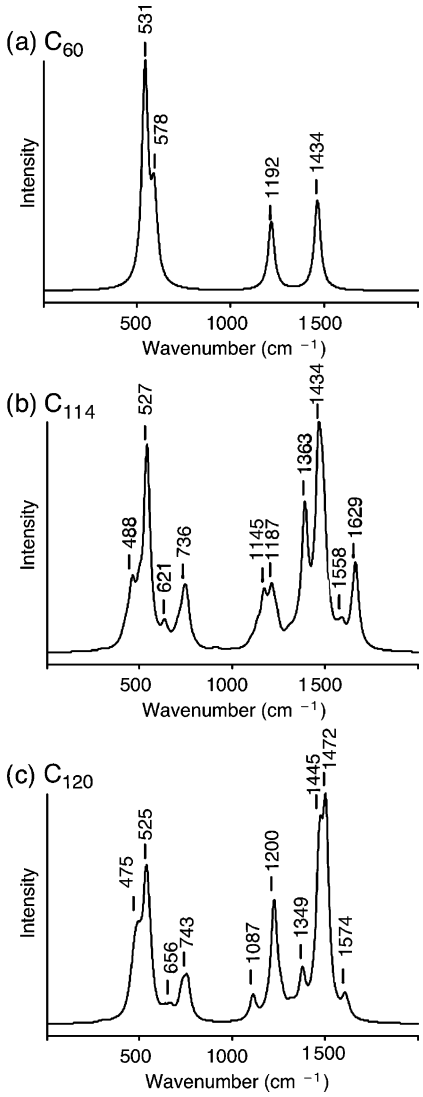

Figure 5. Calculated infrared spectra for the capped tubes (a) C_{60}, (b) C_{114}, and (c) C_{120}.

(34) Because of the A_{1g} symmetry restriction, the number of nodes in the radial motions increases from 0 at an interval of 2.

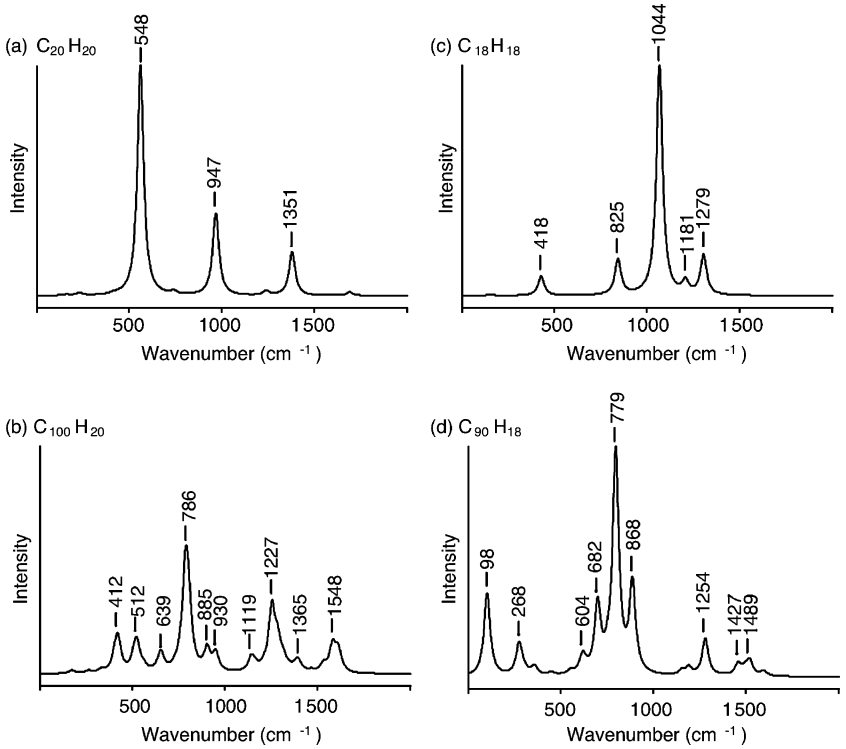

Figure 6. Calculated infrared spectra for the capped tubes (a) $C_{20}H_{20}$, (b) $C_{100}H_{20}$, (c) $C_{18}H_{18}$, and (d) $C_{90}H_{18}$.

modes. We see in Figure 3 that the most size-sensitive modes are the *z*-directed modes, and that their frequency shift in the $C_{20n}H_{20}$ series exceeds ~500 cm^{-1} in the range of $1 \leq n \leq 5$, which is more variant than those for the circumference modes (~100 cm^{-1}). At the same time, the $C_{18n}H_{18}$ series have both C−C stretching *z*-directed and circumference modes that increase and decrease by ~300 cm^{-1} with increasing *n*, respectively. In contrast to the size-sensitive modes, the size-insensitive modes appear in the intermediate-frequency region when $n \geq 2$; the frequencies for the armchair and zigzag series were calculated to be ~780 and ~840 cm^{-1}, respectively. The ^{13}C substitutions in the cylindrical segment of the armchair and zigzag series soften, respectively, the wavenumbers of ~780 and ~ 840 cm^{-1} by ~10 cm^{-1}. The small ^{13}C isotope shifts indicate that the size-insensitive modes have the amplitudes located on the edges. It is, therefore, reasonable that the calculated frequencies do not depend on the cylinder lengths in the tubes.

DFT calculations demonstrate that the vibrational frequencies for the capped tubes are independent of tube length, whereas those in the uncapped tubes are sensitive to the number of chains involved (*n*). The different size dependency is seen in the high-frequency modes that are associated with the tangential motions. Since the tangential modes are well related to the C−C bonding structures in the finite-length nanotubes, the bonding networks should play an important role in determining their frequencies in the high-frequency regions. We can understand the discrepancy in the size dependency between the capped and uncapped tubes from their C−C bonding networks; irrespective of tube length, the capped tubes have similar bond-length alternation patterns within the polyene chains, whereas the uncapped tubes have various bond-deformation patterns. Their bond deformations decline with an increase in the tube length,[12] and therefore, the size dependencies in the high-frequency modes are characteristic of the finite-length tubes. Consequently, the end-cap effects are responsible for their vibrational frequencies in the finite-size tubes.

IR Spectra for the Finite-Length Nanotubes. Taking cognizance of the different size dependency between the capped and uncapped nanotubes, we finally discuss their calculated IR spectra. Figure 5 shows calculated IR spectra for the capped structures C_{60}, C_{114}, and C_{120}. The peaks are broadened by Lorentzian functions, and the IR intensities are normalized to unity for the maximum intensity for each tube. As shown in Figure 5a, C_{60} exhibits four strong IR peaks at 531, 578, 1192, and 1434 cm^{-1}, which are in good agreement with those obtained experimentally.[31] The high-frequency IR-active modes consist of vibrations along tangential directions, and the low-frequency IR-active modes consist of those along radial directions, as shown in Figure S6 (Supporting Information). These intense peaks are identified as the four T_{1u} vibrational modes. In contrast, the symmetry-lowered structure C_{114} (D_{3h} symmetry) has IR-active A_2'' and E' modes, and C_{120} (D_{5d} symmetry) has A_{2u} and E_{1u} modes. Although the symmetry lowering leads to a splitting of the degenerate vibrational modes, the IR spectra for C_{114} and C_{120} have four strong peaks near 530, 1200, and 1440 cm^{-1}, which are comparable to those for C_{60}. The similarity in the IR peak positions of C_{60} and C_{114} (C_{120}) should be attributed to the size insensitivity of their frequencies. Figure 5 shows that relative intensities of the peaks near 1440 cm^{-1} enhance with increasing the tube lengths, whereas those near 530 cm^{-1} remain almost unchanged. The IR intensity, I_i, of vibrational modes, ω_i, is obtained from the derivative of the dipole moment, μ, with respect to the corresponding normal coordinate, Q_i; $I_i \sim |d\mu/dQ_i|^2$. With respect to the tangential modes in the high-frequency regions, the dipole moment increases along the tube lengths to result in increases of IR intensity when *n* is large. On the other hand, the dipole moment

changes on each plane perpendicular to the rotation axis in the radial motions, and hence, it is reasonable that the intensities in the low-frequency regions are independent of tube length.

On the contrary, IR spectra for the uncapped tubes are sensitive to tube length, as shown in Figure 6, where the calculated frequencies ranging from 0 to 2000 cm^{-1} are given. The symmetry labels of the IR-active modes in $C_{20}H_{20}$, $C_{100}H_{20}$, $C_{18}H_{18}$, and $C_{90}H_{18}$ are A_{2u} and E_{1u}. Some peaks are intense: 548, 947, and 1351 cm^{-1} in $C_{20}H_{20}$, and 825, 1044, and 1279 cm^{-1} in $C_{18}H_{18}$. In $C_{20}H_{20}$ and $C_{18}H_{18}$, vibrations with strong IR intensity are located on the C−H bonds on the edges, as shown in Figure S7 (Supporting Information). Increasing the number of chains in the uncapped tubes causes significant changes in their IR spectra, especially intense peak positions. The most intense peak in $C_{100}H_{20}$ appears at 786 cm^{-1}, upshifted by 238 cm^{-1} relative to that in $C_{20}H_{20}$, and in $C_{90}H_{18}$, it appears at 779 cm^{-1}, downshifted by 265 cm^{-1} relative to that in $C_{18}H_{18}$. Therefore, IR peak positions for the uncapped tubes are dependent on tube length, in contrast to those for the capped tubes.

Conclusions

We have analyzed at the B3LYP DFT level of theory the vibrational structures of C_{60}-related tubes C_{40+20n} and C_{42+18n} ($1 \leq n \leq 4$). The tubes terminated by H atoms $C_{20n}H_{20}$ and $C_{18n}H_{18}$ ($1 \leq n \leq 5$) have also been investigated in order to clarify the end-cap effects on the vibrational structures. There are various frequencies in the finite-size tubes, depending on the number of chains involved in the tubes; the tangential vibrational modes appear in 1100−1600 cm^{-1}, the edge state vibrational modes in 700−850 cm^{-1}, and the radial vibrational modes in 300−600 cm^{-1}. The variety of the calculated frequencies in the finite-size tubes is due to the nodal properties of the standing waves. We have demonstrated that the vibrational frequencies for the capped tubes remain almost unchanged with an increase in the number of chains, whereas those for the uncapped tubes are sensitive to tube length. The size insensitivity in the frequencies of the capped tubes comes from the similar bond-length alternation patterns within the *cis*-polyene chains. In contrast, the size sensitivity of the uncapped tubes comes form various bond-deformation patterns. The difference in the vibrational structures between the capped and uncapped tubes can be observed from infrared (IR) analyses; predicted IR spectra for C_{114} and C_{120} are comparable to that for C_{60}, while those for $C_{100}H_{20}$ and $C_{90}H_{18}$ are different from those for $C_{20}H_{20}$ and $C_{18}H_{18}$, respectively.

Acknowledgment. This work has been supported by the 21st Century COE program at Meijo University and jointly with MEXT (Ministry of Education, Culture, Sports, Science and Technology, Japan) and by the "Nanotechnology Support Project" of MEXT at Kyushu University. The support from the Japan Society for the Promotion of Science (JSPS) and Kyushu University P & P "Green Chemistry" (for K.Y.), and the JSPS postdoctoral fellowship (for T.Y.) are gratefully acknowledged.

Supporting Information Available: The vibrational modes with A_{1g} symmetries for the isotope-labeled C_{60}, the $C_{20n}H_{20}$ series, the $C_{18n}H_{18}$ series, the C_{40+20n} series, and the C_{42+18n} series are depicted in Figures S1, S2, S3, S4, and S5, respectively. This material is available free of charge via the Internet at http://pubs.acs.org.

JA0522579